Pergamon

*Atmospheric Environment* Vol. 32, No. 14/15, pp. 2479–2489, 1998

Printed in Great Britain

PII: S1352-2310(98)00021-1

1352-2310/98 $19.00 + 0.00

# THE URBAN PLUME OF VIENNA: COMPARISONS BETWEEN AIRCRAFT MEASUREMENTS AND PHOTOCHEMICAL MODEL RESULTS

GERHARD WOTAWA,*† ANDREAS STOHL‡ and BRUNO NEININGER§

†Institute for Meteorology and Physics (IMP), Universitaet fuer Bodenkultur Wien, Tuerkenschanzstrasse 18, A-1180 Vienna, Austria; ‡Lehrstuhl fuer Bioklimatologie und Immissionsforschung, Ludwig-Maximilians-Universitaet Muenchen, Am Hochanger 13, D-85354 Freising-Weihenstephan, Germany; and §MetAir AG, CH-8308 Illnau, Switzerland

(*First received* 29 *April* 1997 *and in final form* 15 *December* 1997. *Published June* 1998)

**Abstract**—A Lagrangian photochemical box model (IMPO model) developed for ozone forecasts and long-term scenario calculations was evaluated by comparing simulated ozone and nitrogen dioxide concentrations with aircraft measurements done around Vienna/Austria during episodes of high ozone concentrations in 1995. The major aim of these measurements was to record position, extent and intensity of the urban ozone plume. The Lagrangian model simulations were done on a grid covering Vienna and surroundings. The simulated concentrations were interpolated to the aircraft positions. In most cases, the horizontal position of the plume was reasonably well reproduced by the model, demonstrating that despite of all the necessary simplifications, a box model based on air-mass trajectories can be a valuable tool in describing the transport of pollutants. The ozone production in the plume was underpredicted by a factor of 2. High nitrogen dioxide concentrations measured near the city centre were reproduced by the model, but there are strong indications that nitrogen dioxide concentrations were underpredicted by the model in rural areas. A clear quantification proved to be impossible due to uncertainties in the measurement data. © 1998 Elsevier Science Ltd. All rights reserved

*Key word index*: Transport of air pollutants, photochemistry, Lagrangian modelling, ozone, urban plumes.

## 1. INTRODUCTION

Numerical models are essential to understand the complex interactions among emissions, meteorology and atmospheric chemistry. They are widely used to study the formation of ozone ($O_3$) and the behaviour of volatile organic compounds (VOCs). The transport and transformation of air pollutants on regional (10–1000 km) or local (<10 km) scales can be simulated either with Lagrangian trajectory (e.g. Eliassen *et al.*, 1982; De Leeuw *et al.*, 1990; Simpson, 1992) or Eulerian grid models (e.g. Chang *et al.*, 1987; Scherer and Stern, 1989; Builtjes, 1991; Hass, 1991; Moussiopoulos, 1994). Since the processes are complex, nonlinear, interrelated and incompletely understood, model evaluation is indispensable to assess the applicability of the models and the reliability of their results. The model performance can be evaluated by comparing models with measurements (e.g. Jakobs *et al.*, 1995; Hass *et al.*, 1995; Hanna *et al.*, 1996) or by comparing the results of one model with those of others (e.g. Hass *et al.*, 1996).

A Lagrangian photochemical box model, the IMPO model, was developed at the Institute of Meteorology and Physics in Vienna (Stohl *et al.*, 1996a). This model is used for daily ozone forecasts as well as long-term calculations of photooxidant concentrations, which have become possible only due to the simplicity and computational efficiency of the model concept. To assess the reliability of the pollutant transport calculations, a comparison of model simulations with results of aircraft measurements was done.

This paper is divided into six sections. In Section 2, a description of the modelling system and the data assimilation scheme is given. Section 3 provides information on the aircraft measurements. In Section 4, the methods applied for the comparisons between model results and measurements are described. In Section 5, the results of the model evaluation are discussed. Section 6 contains a summary of the main results and the conclusions.

*Author to whom correspondence should be addressed. Tel.: 00 43 1 47058 2033; fax: 00 43 1 470 58 2060; e-mail: wotawa@mail.bo.ku.ac.at.

## 2. MODEL DESCRIPTION

The IMPO model is a Lagrangian photochemical box model. Its basic input are trajectories calculated 96 h backwards in time. Physical and chemical processes are simulated along these trajectories forward in time, yielding the concentrations of chemical species at the receptor location (=starting point of the backward trajectory) for the arrival time (evaluation time).

### 2.1. *Trajectory calculation*

Trajectories are calculated with the FLEXTRA model (Stohl *et al.*, 1995) using data of the weather prediction model of the European Centre for Medium Range Weather Forecasts (ECMWF, 1995). To obtain trajectories representative for boundary-layer transport, a special calculation procedure was developed that averages the wind from the surface to the mixing height during daytime and to the reservoir layer height during nighttime (Stohl and Wotawa, 1995).

Transport processes on a scale of 10 km have to be resolved to adequately simulate the urban pollutant plume of Vienna. The spatial resolution of ECMWF model data (approximately 50 km), however, is too coarse to reproduce the observed variability of the wind fields. Therefore, a diagnostic downscaling technique was developed that corrects ECMWF boundary-layer trajectories by combining ECMWF vertical wind profiles with data of the dense surface wind observation network. A description of the method was published by Stohl *et al.* (1997). It was already shown that the downscaling method yields significantly improved wind analyses at lower levels, and that downscaled trajectories agree much better with constant level balloon trajectories. In this study, it is investigated whether the $O_3$ simulations done with the model are closer to the measurement data if downscaled trajectories are used (see Section 5.1).

### 2.2. *IMPO model description*

The model consists of a vertical column of eight boxes. The lowest box is only 30 m high. Emissions, chemistry, deposition, vertical diffusion and exchange by vertical air motions are calculated. The equations are solved using the quasi-steady-state approximation (QSSA) method as described by De Leeuw (1988).

Anthropogenic emissions across Europe are computed using the EMEP 1991 emission inventory of $150 \times 150$ km resolution (Sandnes, 1993), re-sampled to a resolution of $50 \times 50$ km in Western Europe using the OECD 1980 inventory (Luebkert and De Tilly, 1989). For Central Europe (Austria, Slovakia, Czech Republic and Hungaria), $NO_x$, VOC and CO emissions for the year 1995 are available on a $5 \times 5$ km grid (Winiwarter and Zueger, 1995). VOC emissions from forests are computed depending on land use, temperature and radiation (Lamb *et al.*, 1993; Steinbrecher, 1994), and NO emissions from soils are parameterized according to Williams *et al.* (1992) and Stohl *et al.* (1996b).

The chemical reactions are calculated either with the CBM-IV (Gery *et al.*, 1989) or alternatively with the Euro-RADM mechanism (Stockwell and Kley, 1994). Since CBM-IV offers faster computations, the basic results presented in this study were obtained with this mechanism.

The vertical exchange of pollutants is described by the turbulent diffusion equation using K-theory. Following Yamartino *et al.* (1992), the exchange coefficients are computed using Monin–Obukhov similarity theory in the surface layer and a mixed layer scaling approach in the outer layer (see Troen and Mahrt, 1986; Holtslag *et al.*, 1990). Deposition velocities are calculated applying the resistance method (Wesely, 1989).

The model performance was evaluated for several locations in Austria. It was shown that the IMPO model with CBM-IV chemistry

(i) is able to reproduce daytime concentrations and the mean daily variation of $O_3$, but tends to underpredict daytime $O_3$ concentrations during ozone episodes (Wotawa, 1997);
(ii) tends to underpredict daytime $NO_2$ concentrations (Wotawa, 1997);
(iii) is not very sensitive to changes in its meteorological input data (Wotawa, 1997), but more sensitive to changes in type and length of trajectories or in initial concentrations (Stohl, 1996).

It is the aim of this study to use aircraft measurement data for a comprehensive model evaluation during convective conditions. Model calculations were done on a grid around Vienna with a horizontal resolution of 10 km (Fig. 1). For every grid point, a small-scale IMPO model run along a 12 h backward trajectory was performed. The initial concentrations for the small-scale runs were provided by a single large-scale run along a 84 h trajectory calculated backwards from the centre of the small-scale trajectory positions 12 h before evaluation time. The scale of the model runs is regulated by the air-parcel diameter, which is gradually reduced with decreasing distance from the receptor locations from 500 to 50 km for large- and from 50 to 5 km for small-scale runs. The evaluation time for the grid calculations is 15 CET (Central European Time). All comparisons with measurement data are done using the third model box (100–300 m).

## 3. AIRCRAFT MEASUREMENTS

In 1995, aircraft measurements were conducted around Vienna (MetAir, 1996) as part of the intensive measurement campaign of the Pannonian Ozone

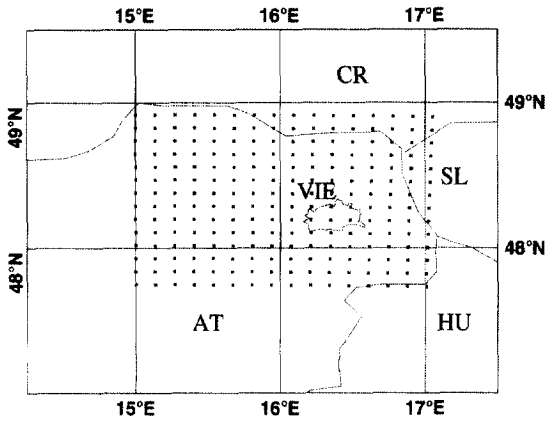


Fig. 1. Grid points (grid distance: 10 km) used as receptor locations for IMPO model runs around Vienna (VIE), Austria (AT). Neighbouring countries Hungaria (HU), Slovakia (SL), Czech Republic (CR).

Project (UBA, 1996). Twenty-six flights on 13 days were done with two instrumented light aircraft. One performed vertical soundings, the other scanned the horizontal pollutant distribution around Vienna. $O_3$ was measured with a UV-photometer (detection limit 2 ppb, range 2–1000 ppb, accuracy 1–2 ppb), $NO_2$ with a LMA-3 luminol-chemoluminecence instrument (detection limit 0.1 ppb, range 0.1–200 ppb, accuracy 0.5–1 ppb). The temperature dependence and the $O_3$ interference of the $NO_2$ data was corrected. A calibration against the transfer standard of the Austrian Environmental Protection Agency was performed. The major problem with the $NO_2$ measurements was the interference with the concentrations of peroxiacetylnitrate (PAN), which leads to an artificial increase of the measured $NO_2$ concentrations. For the type of instrument used, this effect can be estimated as follows: $NO_2 = NO_2 + 0.25$ PAN (see Kelly *et al.*, 1990).

Ten afternoon flights with the horizontally cruising aircraft were selected for model evaluation. The measurement data are available as 1 min averages. The cruising speed of the aircraft was approximately 140 km $h^{-1}$. To eliminate all small-scale variations, the $O_3$, $NO_2$ and position data were transformed into running 15 km averages. Instead of transforming the aircraft measurement data to the model grid, the model results were transformed to the averaged aircraft positions.

Within the well-mixed boundary layer, the concentrations of $O_3$ and $NO_2$ do only slightly depend on the measuring height. Therefore, the influence of varying height was neglected. The temporal evolution of the $O_3$ concentrations during the afternoon was small. Therefore, only a simple correction to the model evaluation time of 15 CET was applied, based on routine surface measurement data available within the area covered by the aircraft.

## 4. METHOD

The following measures are defined for the comparisons between model predicted and observed $O_3$ and $NO_2$ concentrations along the flight route:

(i) *Position error of plume (PEP)*: Distance between the positions of the model predicted $(X_p, Y_p)$ and the observed $(x_p, y_p)$ plume centres. The position of the plume centre is defined here as the averaged position of the highest 5% of the concentrations.

(ii) Radial error of plume: REP $= |D - d|$

$$D = \sqrt{(X_p - X)^2 + (Y_p - Y)^2},$$

$$d = \sqrt{(x_p - X)^2 + (y_p - Y)^2}$$

$D$ is the distance of the predicted and $d$ of the observed plume centre relative to the city centre at location $(X, Y)$.

(iii) Plume position distance ratio: PDR $= D/d$.

(iv) Angular error of plume: AEP $= |\alpha_1 - \alpha_2|$

$$\alpha_1 = \arctan\left(\frac{Y_p - Y}{X_p - X}\right),$$

$$\alpha_2 = \arctan\left(\frac{y_p - Y}{x_p - X}\right)$$

$\alpha_1$ ($\alpha_2$) is the direction of the predicted (observed) plume centre towards the city centre.

(v) Predicted/observed excess concentration of the plume: $\Delta CMOD = C_{80} - C_{20}/\Delta CMES = C_{80} - C_{20}$, $C_{80}/c_{80}$ is the 80th and $C_{20}/c_{20}$ the 20th percentile of the model predicted/measured concentrations. This definition was done to achieve robust results. It was ensured that all findings discussed in the following sections do not depend very much on the definition of the excess concentrations.

(vi) Excess concentration error of the plume: CEP $= |\Delta CMOD - \Delta CMES|$

(vii) Pearson's correlation coefficients $r$ (Press *et al.*, 1992) between the measured and the simulated concentrations of $O_3$ and $NO_2$. From definition, the quantitative interpretation of $r$ requires independent and normally distributed input data. Although air-quality data frequently are neither independent nor normally distributed, $r$ is used for model performance assessment by many authors, mostly in combination with other quantities.

In this study, good model performance is defined according to two criteria: First, $r$ must be greater than 0.6. Secondly, the plume centre position must be described well enough (REP $< 30^c$, $0.7 <$ PDR $< 1.3$).

The following supplementary investigations were done:

The distribution density functions (DDFs) of the model predicted and observed $O_3$ and $NO_2$ concentrations were compared to see whether the model succeeds in reproducing the spatial concentration

distribution. Additionally, statistical relationships between the $O_3$-excess concentrations (actual concentrations minus the 33rd percentiles) and the excess concentrations of $NO_2$ were investigated. These calculations were done for all measurement points not directly affected by new emissions. The selection of measurement points was done according to the modelled ratio $NO_z$ ($NO_y$ minus $NO_x$) to $NO_y$ (total odd nitrogen). All points with $NO_z/NO_y \leq 0.65$ were excluded. The ratio $NO_x/NO_y$ provides a measure of the photochemical age of an air mass (Plummer *et al.*, 1996).

## 5. RESULTS

### 5.1. *Results for ozone*

The correlation criterion ($r > 0.6$) and the plume position criterion (REP < 30°, 0.7 < PDR < 1.3) are fulfilled in six out of 10 cases. In five cases, both criteria are fulfilled (Table 1). As an example, the simulated and measured $O_3$ distribution on 21 July 1995 is shown in Fig. 2. The median of the PEP is 13.9 km, of the AEP 12° and of the REP 6.8 km. Since grid resolution is 10 km, the position results are accurate within the resolution of the simulation. The median value of the PDR is 1.01, indicating that the distance of the plume from the city centre is estimated correctly.

A downscaling method was developed that improves ECMWF windfields in Eastern Austria (see Section 2.1). To see whether this procedure can also improve the $O_3$ simulations, all model runs were repeated with unchanged ECMWF trajectories. As a result, the median of the PEP increased from 13.9 to 21.7 km, the median of the AEP from 12 to 19°, $r$ decreased from 0.66 to 0.51. These results clearly show that the diagnostic downscaling procedure actually improves the $O_3$ simulations done with the IMPO model around Vienna.

On the average, the model underpredicts the background ozone concentrations (Table 2) as well as the concentrations in the plume. The median bias of all simulations is −12 ppb (15%). This result implies that the CBM-IV mechanism underestimates the large-scale ozone formation that produces the background concentrations. Supplemental simulations done with Euro-RADM showed a significantly increased concentration level, the bias changed to +8 ppb. A recent comparison of several mechanisms done by Kuhn *et al.* (1998) demonstrated that Euro-RADM has a substantially increased $O_3$ productivity compared to CBM-IV, which belongs to the least productive mechanisms tested. The difference in the net ozone production is a result of different chemical processes during the nighttime and the early morning hours.

Although the two mechanisms produce different amounts of ozone during simulations of ⩾96 h duration, it was found that both mechanisms produce similar amounts of ozone during daytime. Specifically, both mechanisms underestimate the ozone production in the plume of Vienna during the afternoon. The median of the excess concentrations in the plume is approximately 10 ppb for the measurements, 5 ppb for the CBM-IV and 5.5 ppb for the Euro-RADM simulations.

As a positive feature, it was found that for the day with the highest observed $O_3$ excess concentrations (6 August), the model also predicts the highest excess concentrations. The same is true for the day with the lowest observed $O_3$ excess concentrations (1 August).

A comparison between the DDFs of the predicted and the observed $O_3$ concentrations for all flights is shown in Fig. 3. The predicted DDF shows two different modes, these maximums are shifted towards lower concentrations and the distribution is not as broad as that of the observed concentrations. No explanation has been found for the bimodality of the model

Table 1. Comparison between IMPO model results and aircraft measurements for $O_3$. Position error of plume (PEP, km), radial error of plume (REP, km), plume position distance ratio (PDR), angular error of plume (AEP, degrees), modeled and measured excess concentrations in the plume ($\Delta C_{MOD}$, $\Delta C_{MES}$, ppb), excess concentration error of the plume (CEP, ppb) and correlation coefficient ($r$) between measurements and model results for all flights

| Date | PEP | REP | PDR | AEP | $\Delta C_{MOD}$ | $\Delta C_{MES}$ | CEP | $r$ |
|---|---|---|---|---|---|---|---|---|
| 19950720 | 7.1 | 3.8 | 1.13 | 11 | 5.0 | 6.7 | 1.7 | 0.82 |
| 19950721 | 6.0 | 5.6 | 1.19 | 4 | 6.5 | 6.1 | 0.4 | 0.83 |
| 19950722 | 14.4 | 14.3 | 1.50 | 1 | 4.9 | 7.9 | 3.0 | 0.68 |
| 19950726 | 18.8 | 7.5 | 0.88 | 12 | 5.5 | 14.7 | 9.2 | 0.74 |
| 19950727 | 28.8 | 25.1 | 0.71 | 11 | 7.0 | 13.3 | 6.3 | 0.64 |
| 19950801 | 12.7 | 6.0 | 1.13 | 14 | 2.2 | 5.6 | 3.4 | 0.35 |
| 19950806 | 0.0 | 0.0 | 1.00 | 0 | 10.5 | 17.7 | 7.2 | 0.87 |
| 19950807 | 13.3 | 12.5 | 0.27 | 29 | 2.9 | 13.6 | 10.7 | −0.02 |
| 19950811 | 33.5 | 0.8 | 1.02 | 38 | 3.3 | 9.7 | 6.4 | 0.18 |
| 19950813 | 27.8 | 13.8 | 0.74 | 30 | 4.0 | 11.1 | 7.1 | 0.09 |
| MEDIAN | 13.9 | 6.8 | 1.01 | 12 | 5.0 | 10.4 | 6.4 | 0.66 |

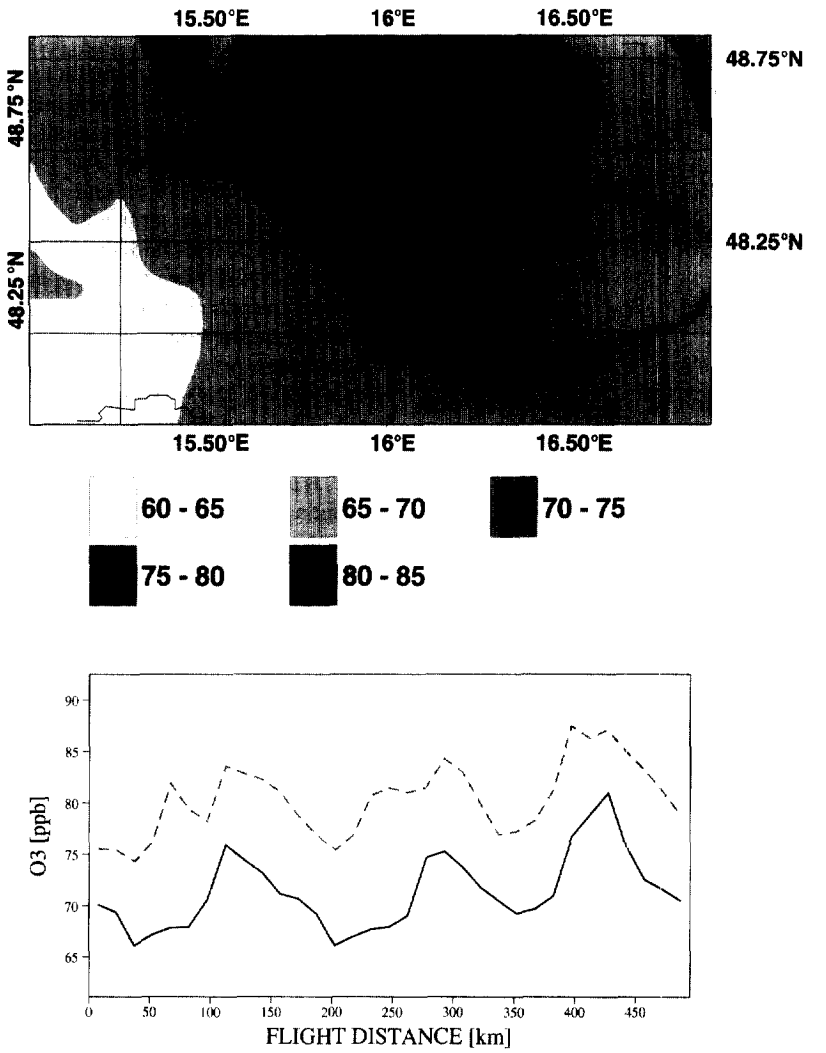


Fig. 2. Top: Contour plot of the area distribution of $O_3$ for 21 July 1995 calculated by the IMPO model. Aircraft measurements are marked with filled symbols. Quadratic symbols denote the highest third, circular symbols the lowest two third of the concentrations. There is a linear increase of symbol height with increasing concentrations. Maximum concentrations are marked. Small quadratic symbols indicate the flight leg. Bottom: Comparison between aircraft measurements (dashed line) and model results of $O_3$ along the flight leg (solid line).

Table 2. Predicted and observed $O_3$ area averages, $O_3$ biases, predicted and observed $NO_2$ area averages and $NO_2$ biases for all flights (all values in ppb). The last row contains the median values of all columns

| Date | $O_{3\,pred}$ | $O_{3\,obs}$ | $O_3$ bias | $NO_{2\,pred}$ | $NO_{2\,obs}$ | $NO_2$ bias |
|---|---|---|---|---|---|---|
| 19950720 | 62.6 | 75.6 | −13.0 | 1.1 | 2.4 | −1.3 |
| 19950721 | 71.3 | 80.4 | −9.1 | 1.2 | 1.2 | −0.0 |
| 19950722 | 70.2 | 81.6 | −11.4 | 0.8 | 1.1 | −0.3 |
| 19950726 | 69.4 | 91.8 | −22.4 | 0.8 | 1.5 | −0.7 |
| 19950727 | 65.3 | 88.4 | −23.1 | 0.8 | 1.1 | −0.3 |
| 19950801 | 72.3 | 83.5 | −11.2 | 0.8 | 1.4 | −0.6 |
| 19950806 | 64.7 | 71.2 | −6.5 | 1.3 | 0.9 | +0.4 |
| 19950807 | 61.2 | 86.0 | −24.8 | 0.8 | 1.9 | −1.1 |
| 19950811 | 64.0 | 87.1 | −23.1 | 1.7 | 2.2 | −0.5 |
| 19950813 | 58.7 | 70.2 | −11.5 | 0.8 | 1.2 | −0.4 |
| MEDIAN | 65.0 | 82.6 | −12.3 | 0.8 | 1.3 | −0.5 |

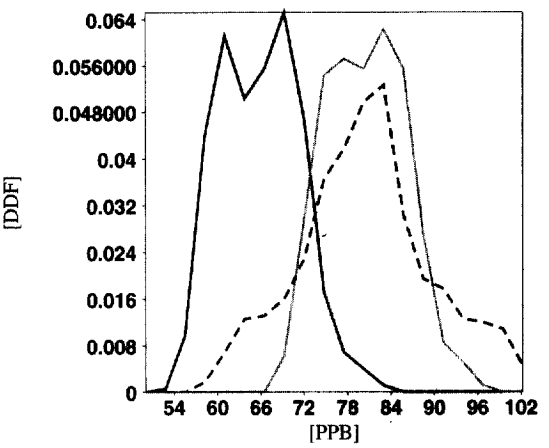


Fig. 3. Distribution density function (DDF) of the predicted (solid line) and observed (dashed line) $O_3$ concentrations during all flights. The bright solid line denotes the DDF of the predicted concentrations after bias correction.

results. After removing the bias of the concentrations by subtracting the difference of the mean values, the Kolmogorov–Smirnov goodness-of-fit test for two samples (as described by Sachs, 1992) applied on the simulated and measured DDF shows that the null hypothesis of equality is rejected on the 1% level, meaning that there is a 1% risk that it is rejected although it is true.

### 5.2. *Results for nitrogen dioxide*

Due to the cross-sensitivity of the $NO_2$ measurements against the concentrations of peroxiacetylnitrate (PAN), the measured concentrations of $NO_2$ are compared to the simulated concentrations of $NO_2$ + 0.25 PAN. Since any erroneous prediction could be attributed to $NO_2$ as well as to PAN, no unambiguous conclusions are possible. Nevertheless, a discussion of results proved to be valuable.

In 6 out of 10 cases, the correlation criterion was fulfilled for $NO_2$ (Table 3). To give an example, the predicted and observed $NO_2$ concentrations on 21 July 1995 are shown in Fig. 4. Since the aircraft directly crossed the urban area in most cases, the REP and the AEP of $NO_2$ are difficult to compare and therefore not investigated in detail, but the predicted position of the $NO_2$ plume was too close to the city centre in most cases. The sum of $NO_2$ + 0.25 PAN was on the average clearly underpredicted by the model (Table 2). This underprediction occurs upwind and downwind of Vienna, but not near the city centre, where the measured concentration peaks are reached or even exceeded (Fig. 4).

A comparison between the DDFs of the predicted and observed $NO_2$ concentrations is shown in Fig. 5. There is a pronounced maximum of the DDF of the predicted $NO_2$ + 0.25 PAN concentrations near 0.8 ppb, whereas the observed DDF is much broader and shows a maximum at about 1.3 ppb. The difference is reduced for concentrations greater than 3 ppb. The Kolmogorov–Smirnov test is applied to compare the DDFs. The hypothesis of equality of the distributions is rejected on the 0.1% level, meaning that an equality of the distributions can almost be ruled out.

### 5.3. *Arguments and possible reasons for $NO_2$ underprediction*

$NO_2$ underprediction is a well-known phenomenon, especially concerning regional scale air quality simulation models (e.g. Simpson, 1992; Hass *et al.*, 1995; Hanna *et al.*, 1996). Due to the uncertainties in the measurements, no unambiguous prove for $NO_2$ underprediction can be supplied in this study. But, as far as the model results are concerned, the sum $NO_2$ + 0.25 PAN is clearly dominated by $NO_2$. A strong argument in favour of $NO_2$ underprediction is provided by the $NO_2$ measurements done at background station Illmitz (16.77° E 47.77° N) situated within the National Park Neusiedlersee south-east of Vienna using a DOAS system, which is able to measure $NO_2$ in the low-ppb range. For all campaign days, the simulated afternoon $NO_2$ concentrations

Table 3. Comparison between IMPO model results and aircraft measurements for $NO_2$. For explanation see also Table 1

| Date | PEP | REP | PDR | AEP | $\Delta C_{MOD}$ | $\Delta C_{MES}$ | CEP | $r$ |
|---|---|---|---|---|---|---|---|---|
| 19950720 | 15.4 | 11.0 | 0.32 | 72 | 0.8 | 0.6 | 0.2 | 0.68 |
| 19950721 | 5.1 | 2.0 | 0.86 | 20 | 0.9 | 0.5 | 0.4 | 0.66 |
| 19950722 | 11.4 | 5.8 | 0.72 | 32 | 0.5 | 0.4 | 0.1 | 0.48 |
| 19950726 | 24.1 | 24.0 | 0.05 | 18 | 0.2 | 1.0 | 0.8 | 0.53 |
| 19950727 | 2.4 | 0.5 | 0.96 | 11 | 0.3 | 0.6 | 0.3 | 0.68 |
| 19950801 | 16.6 | 2.8 | 0.94 | 22 | 0.2 | 0.3 | 0.1 | 0.57 |
| 19950806 | 73.3 | 42.8 | 0.35 | 101 | 0.8 | 0.8 | 0.0 | 0.62 |
| 19950807 | 11.1 | 10.9 | 0.30 | 15 | 0.2 | 1.3 | 1.1 | 0.51 |
| 19950811 | 17.2 | 16.7 | 0.20 | 25 | 1.3 | 1.2 | 0.1 | 0.80 |
| 19950813 | 4.8 | 1.3 | 0.88 | 27 | 0.3 | 0.6 | 0.3 | 0.81 |
| MEDIAN | 13.4 | 8.4 | 0.54 | 24 | 0.4 | 0.6 | 0.3 | 0.64 |

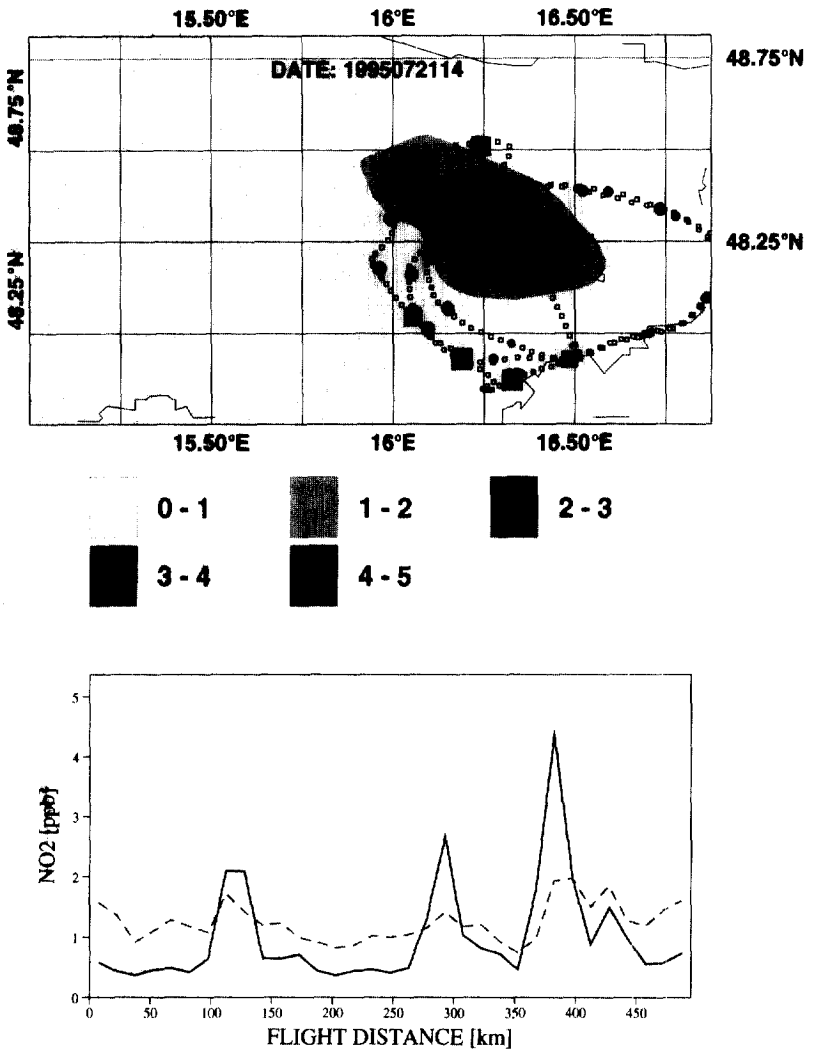


Fig. 4. Top: Contour plot of the area distribution of $NO_2$ + 0.25 PAN for 21 July 1995 calculated by the IMPO model. For explanation see also Fig. 2.

within the lowest model box (surface to 30m) remained well below 0.5 ppb, while the measured afternoon concentrations (3 h averages 12–15 UTC) always exceeded 1.5 ppb.

As the model uncertainty caused by inexact meteorological input data is low during convective weather situations (Wotawa *et al.*, 1997), meteorological reasons for the $NO_2$ underprediction are unlikely. There is no indication that conceptual errors of the Lagrangian box model scheme could explain the differences. Model sensitivity runs with reduced dry deposition velocities of odd nitrogen species showed no large effect. $NO_x$ underprediction in the background area could be caused by an underestimation of $NO_x$ emissions in the whole region. This possibility was checked by performing sensitivity runs assuming higher emissions, but the increase of $NO_x$ emissions necessary to bridge the gap to the measurements was found to be high.

Sub-grid-scale chemical effects are known to cause substantial errors in model predictions (Gillani and Pleim, 1996). The instantaneous dilution of emitted pollutants over one model box is a problematic assumption. Low-$NO_x$ photochemistry (Kleinman, 1994) leads to efficient chemical depletion of $NO_x$, whereas $NO_x$ depletion is slow under high-$NO_x$ conditions. Due to the spatial inhomogeneity of the emissions, $NO_x$ peak concentrations are likely to decrease with increasing box diameter, and consequently the area where low-$NO_x$ conditions predominate changes. Therefore, artificial mixing can lead to $NO_x$- overdepletion. Since the box diameter was chosen in accordance with the resolution of the emission inventory, effects of subgrid chemistry could not be investigated in this study.

Another reason for incorrect model predictions of $NO_2$ might be deficiencies of the chemical schemes in simulating the behaviour of nitric oxides under

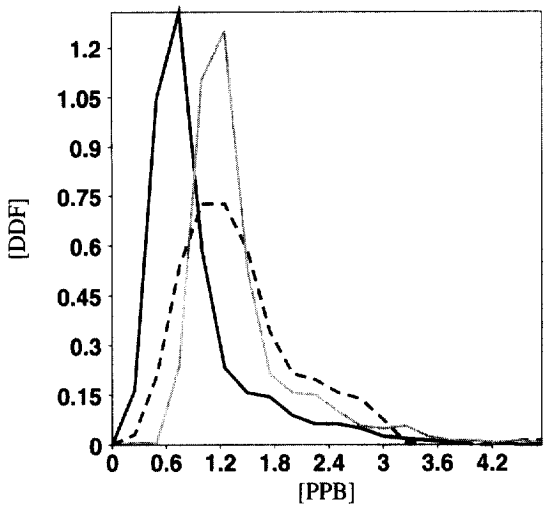


Fig. 5. Distribution density function (DDF) of the predicted (solid line) and observed (dashed line) $NO_2$ ($NO_2$ + 0.25 PAN) concentrations during all flights. The bright solid line denotes the DDF of the predicted concentrations after bias correction.

low-$NO_x$-conditions. A comprehensive investigation of the CBM-IV mechanism was outside the scope of this study, but modelled ratios of $NO_z/NO_y$ are exemplarily studied for one case (July 26) where strong easterly winds occurred in Eastern Austria, leading to increased $O_3$ concentrations 100 km away from Vienna. $NO_2$ concentrations are underpredicted by the model upwind and downwind. The largest bias is found on the lee side, which might partly be explained by increased PAN concentrations disturbing the measurements. The intensity of the ozone plume of Vienna is highly underpredicted, while the horizontal transport direction is estimated very well. In Fig. 6, the modelled ratio $NO_z/NO_y$ is plotted. Low ratios can only be seen close to the city centre. Approximately 30 km downwind, more than 80% of $NO_y$ consists of reaction products, which is typical for a remote site. For instance, in a study describing a rural site in Ontario, Canada, ratios of $NO_z/NO_y$ between 0.6 and 0.8 during the afternoon were reported (Plummer *et al.*, 1996). The CBM-IV mechanism seems to produce an unrealistically fast ageing of the air mass. To check whether this ageing is a specific problem of CBM-IV, model runs were repeated using the Euro-RADM scheme. Euro-RADM performed somewhat more favourable, reducing the $NO_2$ bias and decreasing the ratio $NO_z/NO_y$. But, these improvements were not very large. Anyway, it has to be emphasized that these results do not necessarily indicate shortcomings of the chemical mechanisms. In principle, such results could also, for example, point towards problems with the VOC emission inventory.

### 5.4. *Statistical relationships of* $O_3$ *to* $NO_2$, $NO_z$ *and* VOC

Besides the high-emission areas, low-$NO_x$ concentrations predominate in Eastern Austria. Concentrations between 1 and 2 ppb are measured most frequently. Furthermore, the diagnostic relationship between measured $O_3$ and $NO_2$ excess concentrations outside the urban area was investigated. A simple linear regression model was applied, with $\Delta O_3$ being the dependent and $\Delta NO_2$ being the independent variable. The following results were obtained:

$$\Delta O_3 = 1.6 + 6.9\Delta NO_2 \quad (r = 0.55 \pm 0.02)$$

(Measurements).

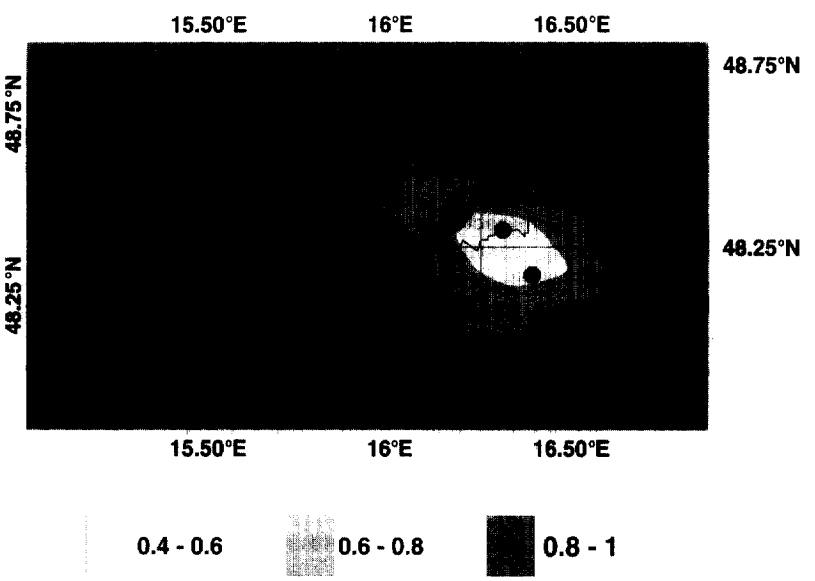


Fig. 6. Contour plot of the area distribution of the ratio $NO_z/NO_y$ (photochemical age of the air masses) for 26 July 1995 as calculated by the IMPO model using the CBM-IV mechanism.

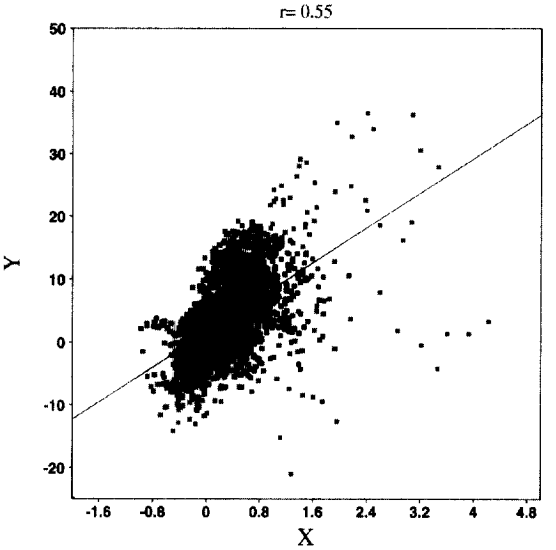


Fig. 7. Scatter plot of the diagnostic relationship between $NO_2$ ($X$-axis) and $O_3$ ($Y$-axis) excess concentrations obseved by the aircraft.

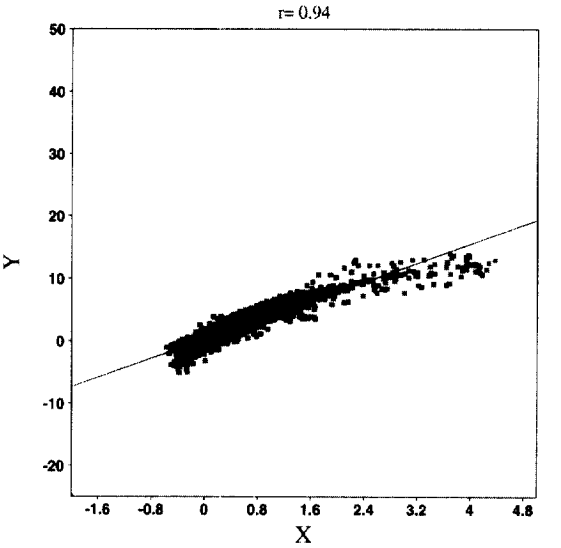


Fig. 8. Scatter plot of the diagnostic relationship between $NO_z$ ($X$-axis) and $O_3$ ($Y$-axis) excess concentrations predicted by the IMPO model.

A scatter plot and the regression line can be seen in Fig. 7. Since a statistical test showed deviations from normal distribution of $\Delta O_3$ and $\Delta NO_2$, the regression results have to be interpreted with caution. Since $NO_z$ concentrations have not been measured and the interpretation of the VOC samples and GC-measurements done is beyond the scope of this study, no conclusions concerning a possible $NO_x$ limitation of the $O_3$ production (see, e.g. Neininger and Dommen, 1996) can be drawn. A comparable relationship between $\Delta O_3$ and $\Delta NO_2$ was observed by Trainer *et al.* (1995) around Birmingham/Alabama (U.S.A.).

To supplement the model evaluation done so far, the diagnostic relationships between simulated $\Delta NO_2$, $\Delta NO_z$, sum of VOCs (ppbC) as independent and $\Delta O_3$ as dependent variable are investigated. A simple linear regression model was applied to model results along the flight leg. The following results are obtained for $\Delta NO_2$:

$$\Delta O_3 = 1.2 + 5.1\ \Delta NO_2 \quad (r = 0.55 \pm 0.02)$$

(Model results).

The slope of the regression line is somewhat less steep than that calculated for the observations.

Since the relationship between $\Delta O_3$ and $\Delta NO_z$ shows the dependence of the $O_3$ concentrations on the $NO_x$ emissions upwind, it gives more profound indications on the efficiency of $O_3$ production caused by $NO_x$:

$$\Delta O_3 = 0.25 + 3.8\ \Delta NO_z \quad (r = 0.94 \pm 0.00)$$

(Model results).

A scatter plot and the regression line can be seen in Fig. 8. A comparable relationship between $\Delta O_3$ and $\Delta NO_z$ was obtained by Roselle and Schere (1995) for the eastern part of the United States using the regional oxidant model (ROM).

At last, the diagnostic relationship between $\Delta O_3$ and $\Delta VOC$ was looked at. Since VOCs partly show a much longer lifetime than $NO_x$ and the transport direction corresponds with that of $O_3$, a positive $r$ value was expected. The following relationship was obtained:

$$\Delta O_3 = 0.36 + 0.46\ \Delta VOC\ (ppbC) \quad (r = 0.83 \pm 0.01)$$

(Model results).

The ratio of $VOC/NO_x$ as simulated by the model is well above 10 within the $O_3$ plume. In the background region, values above 20–100 are calculated. Such ratios are typical for areas where a $NO_x$ limitation of the $O_3$ production is observed. A comparison of modelled to measured ratios of $VOC/NO_x$ would be possible in principle, but was not done in this study.

## 6. SUMMARY AND CONCLUSIONS

An extensive aircraft measurement campaign was done in the year 1995 around Vienna, Austria. Significant ozone production was observed in the urban plume of the city. A simple trajectory-based Lagrangian box model was applied to simulate the conditions observed during the flights. As far as the plume positions and the transport directions are concerned, the model performed favourable. It was demonstrated that reasonable transport simulations on this scale cannot only be obtained using Eulerian grid, but also using Lagrangian box models. The ozone

excess concentrations leeward the city, however, are considerably underpredicted by the model.

Besides the area close to the city centre, low $NO_x$ concentrations were observed. Unfortunately, the $NO_2$ measurements done were disturbed by PAN. The sum of $NO_2 + 0.25$ PAN is clearly underpredicted by the model. There are some arguments in favour of an $NO_2$ underprediction upwind and downwind of Vienna, but this can not be proved unambiguously. Using CBM-IV chemistry, surprisingly high ratios of $NO_z/NO_y$ are modelled. These ratios are somewhat reduced using the Euro-RADM scheme. Unfortunately, no observations of $NO_y$ are available.

Further analysis of the measurements showed that there is a positive relationship between the excess concentrations of $O_3$ and $NO_2$. The correlation coefficient has to be interpreted cautiously due to the non-normality of the data set. Based on the measurements available, a limitation of the $O_3$ production by $NO_x$ can neither be assumed nor rejected. Analyses of model results showed strong linear relationships between the excess concentrations of $O_3$ and its precursors ($NO_z$, VOC). The strong relationship between $O_3$ and the $NO_z$ compounds and the surprisingly high ratios of VOC to $NO_x$ indicate that the modelled $O_3$ production could be $NO_x$ limited.

*Acknowledgements*—Parts of this study and the aircraft measurements were funded by the Austrian Federal Ministries of Science, Environment and Agriculture and the governments of the Countries Vienna, Lower Austria and Burgenland as part of the Pannonian Ozone Project (POP). The model studies are based on the data of the European Centre of Medium Range Weather Forecasts (ECMWF) in Reading, UK and the Central Institute of Meteorology and Geodynamics in Vienna, Austria. The emission inventory for Austria, Czech Republic, Slovakia and Hungaria has been contributed by the Austrian Research Centre Seibersdorf. The POP measurement campaign was supported by the Austrian Environmental Protection Agency (Umweltbundesamt) in Vienna. The authors want to express thanks to all these organisations and their representatives. Last but not least, the authors are grateful to two anonymous referees for their valuable comments and suggestions.

## REFERENCES

Builtjes, P. J. H. (1991) The LOTOS model results. In: *Comparison of Three Models for Long Term Photochemical Oxidants in Europe*. ed. T. Iversen EMEP/MSC-W Report 3/91, MSC-W, Oslo, Norway.

Chang, J. S., Brost, R. A., Isaksen, I. S. A., Madronich, S., Middleton, P., Stockwell, W. R. and Walcek, C. J. (1987) A three dimensional Eulerian acid deposition model: Physical concepts and formulation. *Journal of Geophysical Research* **92**, 14,681–14,700.

De Leeuw, F. A. A. M. (1988) *Numerical Solution of Ordinary Differential Equations Arising from Chemical Kinetics*. National Institute of Public Health and Environmental Protection (RIVM), Report 228603005, Bilthoven, The Netherlands.

De Leeuw, F. A. A. M., Van Rheineck Leyssius, H. J. and Builtjes, P. J. H. (1990) Calculation of long term averaged ground level ozone concentrations. *Atmospheric Environment* **24A**, 185–193.

Eliassen, A., Hov, O., Isaksen, I. S. A., Saltbones, J. and Stordal, F. (1982) A Lagrangian long-range transport model with atmospheric boundary layer chemistry. *Journal of Applied Meteorology* **21**, 1645–1661.

European Centre for Medium Range Weather Forecasts (ECMWF, 1995) *User guide to ECMWF Products 2.1*. ECMWF, Reading, U.K.

Gery, M. W., Whitten, G. Z., Killus, J. P. and Dodge, M. C. (1989) A photochemical kinetics mechanism for urban and regional scale computer modeling. *Journal of Geophysical Research* **94**, 12,925–12,956.

Gillani, N. V. and Pleim, J. E. (1996) Sub-grid-scale features of anthropogenic emissions of $NO_x$ and VOC in the context of regional Eulerian models. *Atmospheric Environment* **30**, 2043–2059.

Hanna, S. R., Moore, G. E. and Fernau, M. E. (1996) Evaluation of photochemical grid models (UAM-IV, UAM-V, and the ROM/UAM-IV couple) using data from the Lake Michigan Ozone Study (LMOS). *Atmospheric Environment* **30**, 3265–3279.

Hass, H. (1991) Description of the EURAD chemistry transport module (CTM) version 2. In: *Report 83*, eds. A. Ebel *et al.* Institute of Geophysics and Meteorology, University of Cologne, Germany.

Hass, H., Builtjes, P. J. H., Simpson, D. and Stern, R. (1996) Comparison of photooxidant dispersion model results. *Special EUROTRAC Report*, Garmisch Partenkirchen, Germany.

Hass, H., Jakobs, H. J. and Memmesheimer, M. (1995) Analysis of a regional model (EURAD) near surface gas concentration predictions using observations from networks. *Meteorological Atmospheric Physics* **57**, 173–200.

Holtslag, A. A. M., De Bruijn, E. I. F. and Pan, H. L. (1990) A high resolution air mass transformation model for short-range weather forecasting. *Monthly Weather Review*. **118**, 1561–1575.

Jakobs, H. J., Feldmann, H., Hass, H. and Memmesheimer, M. (1995) The use of nested models for air pollution studies: an application of the EURAD model to an SANA episode. *Journal of Applied Meteorology* **34**, 1301–1319.

Kelly, T. J., Spicer, C. W. and Ward, G. F. (1990) An assessment of the luminol chemiluminescence technique for measurement of the $NO_2$ in ambient air. *Atmospheric Environment* **24A**, 2397–2404.

Kleinman, L. I. (1994) Low and high $NO_x$ tropospheric photochemistry. *Journal of Geophysical Research* **99**, 16,831–16,838.

Kuhn, M., Builtjes, P. J. H., Poppe, D., Simpson, D., Stockwell, W. R. *et al.* (1998) Intercomparison of the gas-phase chemistry in several chemistry and transport models. *Atmospheric Environment* **32**, 693–709.

Lamb, B., Gay, D., Westberg, H. and Pierce, T. (1993) A biogenic hydrocarbon emission inventory for the USA using a simple forest canopy model. *Atmospheric Environment* **27A**, 1673–1690.

Luebkert, P. and De Tilly, S. (1989) The OECD-MAP emission inventory for $SO_2$, $NO_X$ and VOC in Western Europe. *Atmospheric Environment* **23**, 3–15.

MetAir (1996) *Schlußbericht zu den Flugmessdaten für das Pannonische Ozonprojekt (POP-95)*. Im Auftrag des Bundesministeriums für Umwelt der Republik Österreich. Austrian Federal Ministry for the Environment, Vienna, Austria.

Moussiopoulos, N. (1994) MARS-Model for atmospheric dispersion of reactive species. In *The EUMAC Zoming Model, Model Structure and Applications*, ed. N. Moussiopoulos. Special EUROTRAC Report, Garmisch Partenkirchen, Germany.

Neininger, B. and Dommen, J. (1996) *POLLUMET: Luftverschmutzung und Meteorologie in der Schweiz.*

Bundesamt fuer Umwelt, ed. Wald und Landschaft, Report "Umwelt-Materialien Nr. 63, Luft", Berne, Switzerland.

Plummer, D. A., McConnell, J. C., Shepson, P. B., Hastie, D. R. and Niki, H. (1996) Modeling of ozone formation at a rural site in southern Ontario. *Atmospheric Environment* **30**, 2195–2217.

Press, W. H., Teukolsky, S. A., Vetterling, W. T. and Flannery, B. P. (1992) *Numerical Recipes in FORTRAN. The Art of Scientific Computing*, 2nd ed. Cambridge University Press, New York, U.S.A.

Roselle, S. J. and Schere, K. L. (1995) Modeled response of photochemical oxidants to systematic reductions in anthropogenic volatile organic compound and $NO_x$ emissions. *Journal of Geophysical Research* **100** (D11), **22**, 929–22,941.

Sachs, L. (1992) *Angewandte Statistik*. 7. Issue, ISBN 3-540-52085-6, Springer, Berlin, Germany.

Sandnes, H. (1993) *Calculated budgets for airborne acidifying components in Europe, 1985, 1987, 1988, 1989, 1990, 1991 and 1992*. EMEP MSC-W Report 1/93, MSC-W, Oslo, Norway.

Scherer, B. and Stern, R. (1989) Simulation of an acid deposition episode over Europe with the TADAP/ADOM Eulerian regional model. In: *Air Pollution Modeling an its Application VII*, ed. H. Van Dop. Plenum Press, New York, USA.

Simpson, D. (1992) Long-period modelling of photochemical oxidants in Europe. Model calculations for July 1985. *Atmospheric Environment* **26A**, 1609–1634.

Steinbrecher, R. (1994) Emission of VOCs from Selected European Ecosystems: the State of the Art. In: *The Proceedings of EUROTRAC Symposium 1994*, ed. Borell *et al.* SPB Academic Publishing, The Hague, The Netherlands.

Stockwell, W. R. and Kley, D. (1994) *The Euro-RADM Mechanism. A Gas-Phase Chemical Mechanism for European air Quality Studies*. Berichte des Forschungszentrums Juelich 2686, Research Centre Jülich, Germany, 114 pp.

Stohl, A. (1996) On the use of trajectories for establishing source-receptor relationships of air pollutants. Doctoral thesis, Institute of Meteorology and Geophysics, University of Vienna, Vienna, Austria.

Stohl, A. and Wotawa, G. (1995) A method for computing single trajectories representing boundary layer transport. *Atmospheric Environment* **29**, 3235–3238.

Stohl, A., Baumann, K., Wotawa, G., Langer, M., Neininger, B., Piringer, M. and Formeyer, H. (1997) Diagnostic downscaling of large scale wind fields to compute local scale trajectories. *Journal of Applied Meteorology* **36**, 931–942

Stohl, A., Wotawa, G. and Kromp-Kolb, H. (1996a) The IMPO modeling system—description, sensitivity studies and applications. Final report of the Institute for Meteorology and Physics for the Pannonian Ozone Project. Institute for Meteorology and Physics, Vienna, Austria.

Stohl, A., Williams, E., Wotawa, G. and Kromp-Kolb, H. (1996b) Nitrogen oxides emissions from soils and their effect on the photochemical formation of ozone in Europe. *Atmospheric Environment* **30**, 3741–3755.

Stohl, A., Wotawa, G., Seibert, P. and Kromp-Kolb, H. (1995) Interpolation errors in wind fields as a function of spatial and temporal resolution and their impact on different types of kinematic trajectories. *Journal of Applied Meteorology* **34**, 2149–2165.

Trainer, M., Ridley, B. A., Buhr, M. P., Kok, G., Walega, J., Hübler, G., Parrish, D. D. and Fehsenfeld, F. C. (1995) Regional ozone and urban plumes in the southeastern United States: Birmingham, a case study. *Journal of Geophysical Research* **100**(D9), 18,823–18,834

Troen, I. B. and Mahrt, L. (1986) A simple model of the atmospheric boundary layer: sensitivity to surface evaporation. *Boundary-Layer Meteorology* **37**, 129–148.

Umweltbundesamt/Austrian Environmental Protection Agency (UBA, 1996) *Pannonisches Ozonprojekt (POP). Teilprojekt "Daten & Experimente"*. Report UBA-95-120. Umweltbundesamt, Vienna, Austria.

Wesely, M. L. (1989) Parameterization of surface resistances to gaseous dry deposition in regional-scale numerical models. *Atmospheric Environment* **23A**, 1293–1304.

Williams, E. J., Guenther, A. and Fehsenfeld, F. C. (1992) An inventory of nitric oxide emissions from soils in the United States. *Journal of Geophysical Research* **97**, 7511–7519.

Winiwarter, W. and Zueger, J. (1995) *Pannonisches Ozonprojekt. Teilprojekt Emissionen*. Report OEFZS-A-3601, Austrian Research Center Seibersdorf, Seibersdorf, Austria.

Wotawa, G. (1997) Analyse und Modellierung von Ozon und anderen Luftschadstoffen in Ostösterreich. Doctoral thesis, Institute of Meteorology and Geophysics, University of Vienna, Vienna, Austria.

Wotawa, G., Stohl, A. and Kromp-Kolb, H. (1997) Estimating the uncertainty of a Lagrangian photochemical air quality simulation model caused by inexact meteorological input data. *Reliability Engineering and System Safety* **57**, 31–40.

Yamartino, R. J., Scire, J. S., Charmichael, G. R. and Chang, Y. S. (1992) The CALGRID mesoscale photochemical grid model - I. Model formulation. *Atmospheric Environment* **26A**, 1493–1512.